Met O 11 Technical Note No 189

INTERIOR LAYERS IN THE ATMOSPHERE - THEORETICAL AND COMPUTATIONAL ASPECTS

by

M.J.P. Cullen

This paper was presented at the BAIL III Conference on Boundary and interior layers. Dublin 20th June - 22nd June 1984.

Met O 11 (Forecasting Research Branch)
Meteorological Office,
London Road,
Bracknell,
Berkshire,
England.

June 1984.

INTERIOR LAYERS IN THE ATMOSPHERE - THEORETICAL AND COMPUTATIONAL ASPECTS

M.J.P. Cullen

Meteorological Office, London Road, Bracknell, Berkshire, RG12 2SZ, UK

The most obvious example of an interior shear layer in the atmosphere is a front, which forms the boundary between air masses of differing characteristics. An appropriate form of the governing equations is derived by a scaling argument. A closed solution of these equations can be constructed using piecewise constant initial data. These solutions can contain fronts. The scaling is then re-examined in the neighbourhood of fronts and shown to be consistent if no fluid crosses the front and there is no pressure jump. In simple cases actual solutions can be derived by geometrical methods given piecewise constant data. These solutions are then used to test finite difference methods. It is found that solutions of the scaled governing equations converge to the geometrical solution, albeit slowly. However, if the primitive form of the equations are used, convergence is to a different solution. The difference can be related to the different boundary conditions necessary if the equations are scaled.

The final detailed version of this paper will be submitted for publication elsewhere.

1. Introduction

Extensive work on the mathematical theory of fronts has been carried out in the last few years, much of it is reviewed by Hoskins (1982). The computational aspects have not received so much attention, and most standard discussions of numerical methods for meteorological problems assume that the solutions are smooth (Haltiner and Williams (1980)). In other areas of computational fluid dynamics, correct treatment of discontinuities is essential if good results are to be obtained. It is therefore natural to ask what rules have to be obeyed to model meteorological fronts properly. The problem is difficult because many fronts drawn on weather maps are merely regions of somewhat enhanced temperature gradient rather than near-discontinuities. In other cases they are very sharp. In addition, fronts slope in the vertical and the amount of slope is one of the important parameters. Fig. 1 shows a section of a typical weather map, simplified from Buzzi and Tibaldi (1978). This map contains isopleths of mean sea level pressure. Fronts appear as waving lines on the map. These lines represent the intersection of the front with the surface.

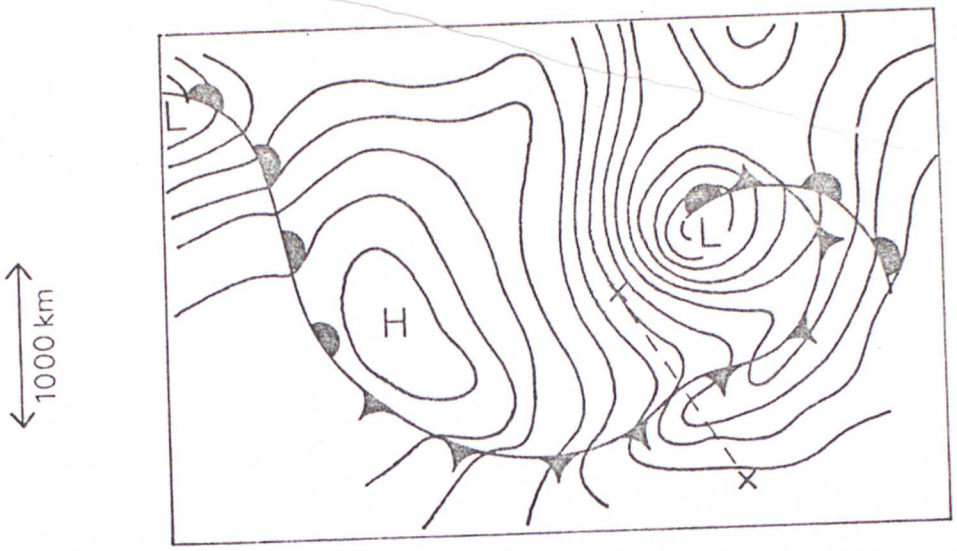

Fig. 1: Typical surface pressure map with cold fronts (▲▲) and warm fronts (◠◠)

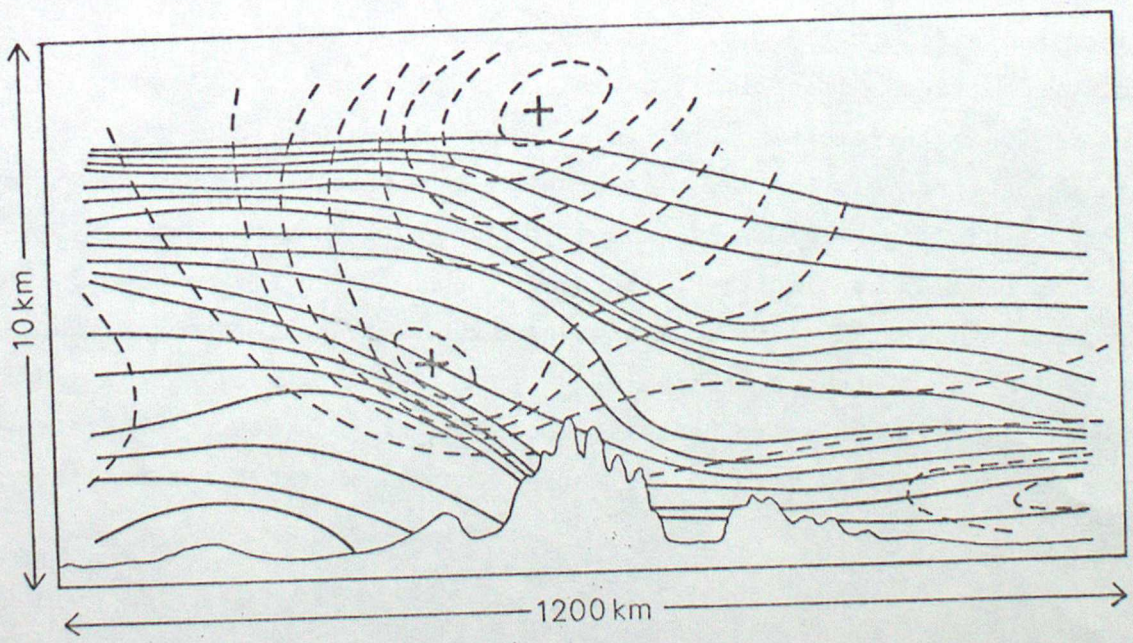

Fig. 2: Cross section through front along dashed line in Fig. 1. Solid lines are contours of potential temperature, dashed lines contours of long-front wind.

The vertical structure is shown in Fig. 2. This cross section is along the dashed line in Fig. 1 and shows the potential temperature (the temperature of the air if transported adiabatically to a standard pressure) and the wind component parallel to the front.

It is clearly seen from Fig. 2 that the long-front wind increases most rapidly in the vertical when the isentropes slope down to the right. This allows the pressure gradient due to the buoyancy gradient to balance the Coriolis acceleration due to the earth's rotation. The slope of a frontal surface is thus a crucial part of its dynamics and a front cannot be treated as a purely one-dimensional phenomenon. In this paper we derive solutions containing sloping discontinuities from a scaled form of the governing equations and discuss methods of computing them.

2. Governing equations

These are derived from the standard equations of motion for a perfect gas. We initially ignore frictional effects and assume that the motion is adiabatic. Effects of water vapour are very important in real fronts, but require entirely different treatment. It is usual to make the hydrostatic assumption, which is accurate to about 1 in 10^6 on the scales shown in Figs 1 and 2. This gives:

$$\frac{Du}{Dt} - fv + \frac{1}{\rho}\frac{\partial p}{\partial x} = 0 , \tag{1}$$

$$\frac{Dv}{Dt} + fu + \frac{1}{\rho}\frac{\partial p}{\partial y} = 0 , \tag{2}$$

$$g + \frac{1}{\rho}\frac{\partial p}{\partial z} = 0 , \tag{3}$$

$$\frac{D\rho}{Dt} + \rho\left(\frac{\partial u}{\partial x} + \frac{\partial v}{\partial y} + \frac{\partial \hat{w}}{\partial \hat{z}}\right) = 0 , \tag{4}$$

$$\frac{D\theta}{Dt} \equiv \frac{\partial \theta}{\partial t} + u\frac{\partial \theta}{\partial x} + v\frac{\partial \theta}{\partial y} + \hat{w}\frac{\partial \theta}{\partial \hat{z}} = 0 , \tag{5}$$

$$\rho^{-1} = \theta P'(p) , \qquad P = p^{(\gamma-1)/\gamma} , \tag{6}$$

$$\hat{w} = 0 \quad \text{at} \quad \hat{z} = 0 . \tag{7}$$

where $(u, v, \hat{w})$ are velocity components in local Eulerian coordinates with the $\hat{z}$ axis vertical. p is pressure, θ potential temperature or entropy, ρ density, f the Coriolis parameter, g the acceleration due to gravity.

These equations can be transformed into a system which resembles the equations governing an incompressible fluid by first of all changing variables to use (t, x, y, p) as independent variables and $u, v, \omega = \frac{Dp}{Dt}$, $\phi = g\hat{z}$ and θ as dependent variables. The details are set out in Haltiner and Williams (1980). Then a further transformation can be made in the p coordinate to an independent variable

$$z = \left(1 - (p/\bar{p})^{(\gamma-1/\gamma)} \right) \frac{\gamma}{\gamma-1} H_s \tag{8}$$

where $H_s = \bar{p}/\bar{\rho}g$ and $\bar{p}$ and $\bar{\rho}$ are reference values of pressure and density. This transformation makes z equal to the physical height $\hat{z}$ in an adiabatic atmosphere. The use of this coordinate means that $z = \gamma H_s/\gamma-1$ at $p = 0$ and an upper boundary condition can be imposed

$$w = \frac{Dz}{Dt} = 0 \quad \text{at} \quad z = \gamma H_s/\gamma-1 \tag{9}$$

This transformation is discussed in detail by Hoskins and Bretherton (1972). We now make the Boussinesq approximation, which gives the system

$$\frac{Du}{Dt} - fv + \frac{\partial \phi}{\partial x} = 0 \tag{10}$$

$$\frac{Dv}{Dt} + fu + \frac{\partial \phi}{\partial y} = 0 \tag{11}$$

$$g\theta/\bar{\theta} + \frac{\partial \phi}{\partial z} = 0 \tag{12}$$

$$\frac{\partial u}{\partial x} + \frac{\partial v}{\partial y} + \frac{\partial w}{\partial z} = 0 \tag{13}$$

$$\frac{D\theta}{Dt} = 0 \tag{14}$$

$$w = 0 \quad \text{at} \quad z = \gamma H_s/\gamma-1 \tag{15}$$

For the purposes of this paper we approximate the lower boundary condition by

$$w = 0 \quad \text{at} \quad z = 0 \tag{16}$$

and assume that f is constant.

This neglects the effect of surface pressure variations on the boundary condition. Both these approximations are for understanding only, and are not made in actual computations. Comparison with the system (1) to (5) shows that the transformations have converted the equations into those of an incompressible Boussinesq fluid within rigid boundaries.

3. Scale analysis

Understanding of the solution of (10) to (15) depends on recognising that the forcing terms g and $f\underline{u}$ are large compared to the corresponding accelerations. The large size of g has already been accounted for by making the hydrostatic approximation. The size of $f\underline{u}$ is measured by the Rossby number

$$\epsilon = \left| \frac{D\underline{u}}{Dt} \right| / |f\underline{u}| \qquad (17)$$

When expressed in this form, even for extreme large scale weather events ϵ only reaches a value of about 1/6. This value was calculated for the level of maximum wind in association with the explosive development of a storm over the USA (Uccelini et al (1984)). However, if ϵ is calculated from typical length scales and velocities on a weather map such as Fig. 1, it is quite easy to reach $O(1)$ values. The difference is because strong flows in the atmosphere tend to be parallel to the strong gradients, so that $D\underline{u}/Dt$ is much smaller than might be expected.

Expanding (10) to (15) in powers of ϵ gives, setting $u = u_0 + \epsilon u_1$, etc;

to $O(1)$:

$$-fv_0 + \frac{\partial \phi_0}{\partial x} = 0 , \qquad (18)$$

$$fu_0 + \frac{\partial \phi_0}{\partial y} = 0 , \qquad (19)$$

$$g\theta/\bar{\theta} + \frac{\partial \phi_0}{\partial z} = 0 , \qquad (20)$$

whence

$$\frac{\partial u_0}{\partial x} + \frac{\partial v_0}{\partial y} = 0 ; \qquad (21)$$

so

$$w_0 = 0 .$$

To $O(\epsilon)$

$$\frac{Du_0}{Dt} - fv_1 + \frac{\partial \phi_1}{\partial x} = 0 \qquad (22)$$

$$\frac{Dv_0}{Dt} + fu_1 + \frac{\partial \phi_1}{\partial y} = 0 \qquad (23)$$

$$g\theta_1/\bar{\theta} + \frac{\partial \phi_1}{\partial z} = 0 \qquad (24)$$

$$\frac{\partial u_1}{\partial x} + \frac{\partial v_1}{\partial y} + \frac{\partial w_1}{\partial z} = 0 \qquad (25)$$

$$\frac{D\theta}{Dt} = 0 \qquad (26)$$

In order to ensure uniform validity of the expansion for times of O(1) it is necessary to approximate the trajectory to one order higher, so we set

$$\frac{D}{Dt} = \frac{\partial}{\partial t} + (u_0 + \epsilon u_1)\frac{\partial}{\partial x} + (v_0 + \epsilon v_1)\frac{\partial}{\partial y} + w_1 \frac{\partial}{\partial z} \qquad (27)$$

System (22) to (26) form the semigeostrophic equations used by Hoskins and others in various papers, reviewed in Hoskins (1982). We consider these as "outer" equations of the problem and study their solutions.

4. Solution of outer problem

It has been shown by Hoskins and Draghici (1977) that the system (22) to (26) can be rewritten as a set of Lagrangian conservation laws.

Define

$$fu_g = -\partial\phi/\partial y \,, \quad fv_g = \partial\phi/\partial x \,, \quad M = v_g + fx, \quad N = -u_g + fy \qquad (28)$$

Let the region of solution in (x,y) be Ω, with boundary $\partial\Omega$. Let Ω be convex Then

$$\frac{DM}{Dt} = fu_g \qquad (29)$$

$$\frac{DN}{Dt} = fv_g \qquad (30)$$

$$\frac{D\theta}{Dt} = 0 \qquad (31)$$

$$\frac{\partial u}{\partial x} + \frac{\partial v}{\partial y} + \frac{\partial w}{\partial z} = 0 \qquad (32)$$

$$w = 0 \quad \text{at} \quad z = 0,\ \gamma H_s/\gamma - 1 \qquad (33)$$

$$\underline{u}\cdot\underline{n} = 0 \quad \text{on} \quad \partial\Omega \qquad (34)$$

$$(fM,\ fN,\ g\theta/\tilde{\theta}) = (\partial P/\partial x,\ \partial P/\partial y,\ \partial P/\partial z) \qquad (35)$$

where

$$P = \phi + \tfrac{1}{2}f^2(x^2 + y^2)$$

It has been shown by Cullen and Purser (1984) that this problem can be solved by approximating the initial data by piecewise constants: Start with n "elements" with associated constant values (M_n, N_n, θ_n) and volumes τ_n at $t = 0$. Fig. 3 shows a possible configuration in two dimensions.

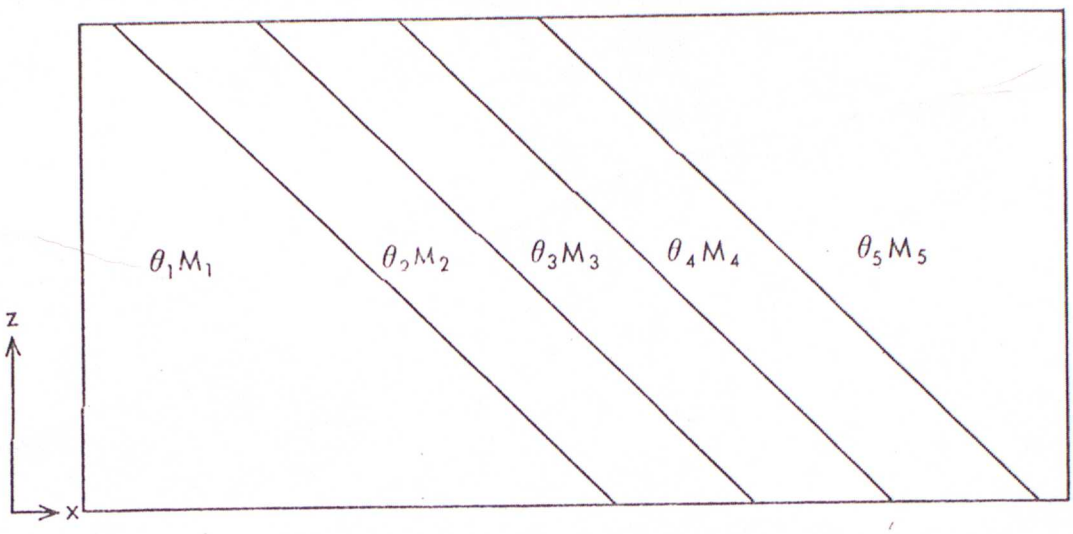

Fig. 3: Piecewise constant data for two-dimensional semi-geostrophic equations.

To update the solution in time we increment the values of M and N in each element according to (29) and (30). The velocity field (u, v, w) is determined implicitly by the need to satisfy (34). The only effect of this velocity is to rearrange the elements, preserving the values of M, N, θ and the volumes τ_n. The existence of the necessary rearrangement has been shown by Cullen and Purser (1984) in the following terms.

Definition — A solution of (29) to (35) characterized by the values of the function $P(x,y,z,t)$ on Ω is dynamically stable if the Hessian matrix $\left(\partial^2 P/\partial x_i \partial x_j\right)$ has no negative eigenvalues. For non-smooth solutions this is generalised to requiring the region in $\mathbb{R}^4$: $(S \geq P(x,y,z), \underline{x} \in \Omega)$ to be convex.

Remark — If the Hessian does have negative eigenvalues small peturbations to the solution can grow and large accelerations will be generated, violating the scaling assumptions in section 3, (Hoskins, (1974)).

Theorem — There is a unique arrangement of fluid elements with given values (M_n, N_n, θ_n), volumes τ_n, satisfying (34) everywhere that is dynamically stable.

Proof — See Cullen and Purser (1984). The convex surface corresponding to the data in Fig. 3 is shown in Fig. 4.

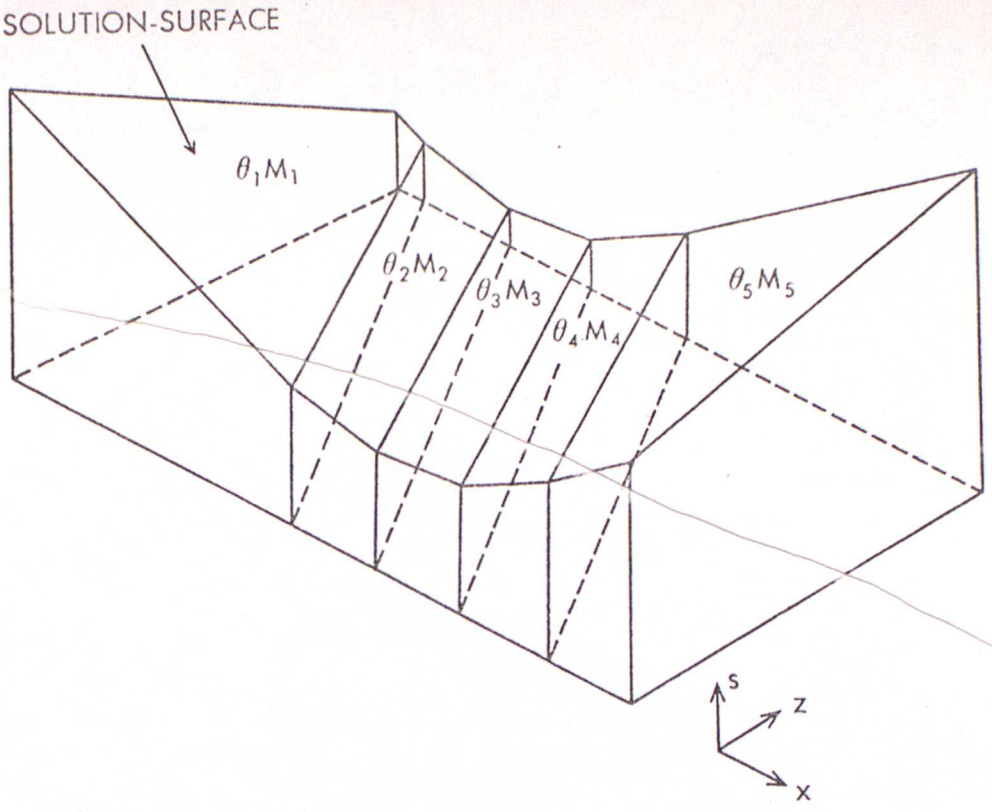

Fig. 4: Convex surface $S = P(x,y)$ corresponding to data in Fig. 3.

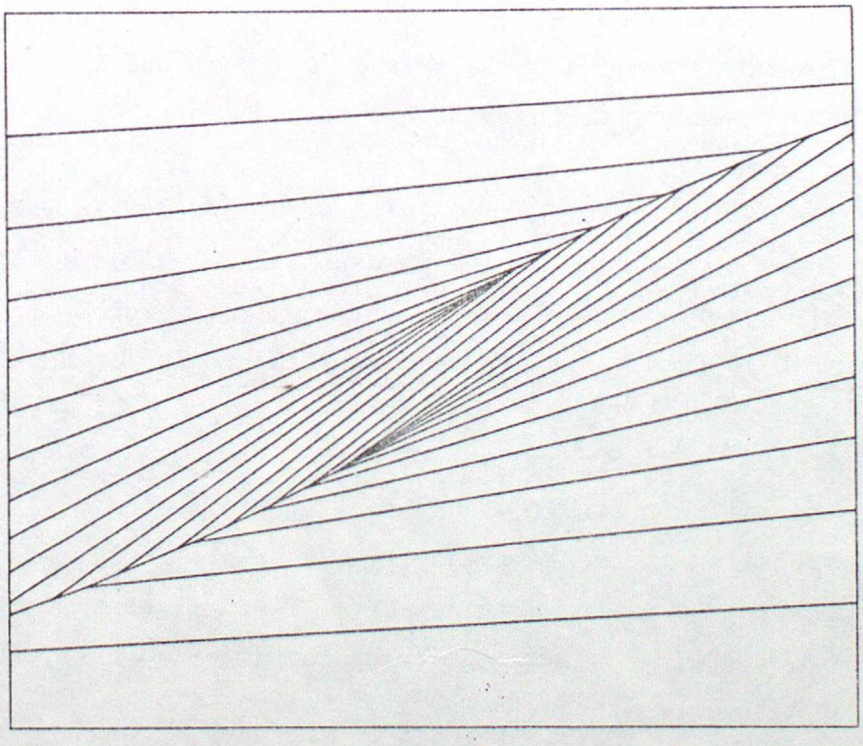

Fig. 5: Solution for piecewise constant data containing a front.

It is clear that there is no reason in general why the solution for M, N and θ should be continuous, though P must be continuous. Fig. 5 is an example of a

solution with a finite discontinuity.

The nature of discontinuities is restricted by the conservation of the potential vorticity

$$q = \frac{\partial(N, -M, \theta)}{\partial(x, y, z)} \tag{36}$$

following the motion. q is essentially the Gaussian curvature of the surface $s = P(x,y,z)$. A discontinuity in ∇P corresponds to a fold in this surface, which can only be reconciled with finite q if the discontinuity intersects the boundary of Ω. Otherwise the circulation integral $\int q \cdot dl$ round the discontinuity would not tend to zero as the contour was shrunk, implying infinite curvature.

The solution is not unique if Ω is non-convex. This turns out to be a possible explanation of some aspects of mountain flows.

5. Definition of inner problem

The results of section 4 indicate that the outer solution can produce regions of discontinuity, but their nature is restricted by the conservation of q and the convexity of $P(x,y,z)$. It is now necessary to rescale near the discontinuity where ϵ may not be small. In general the surface of discontinuity will satisfy the equations

$$\frac{dz}{dx} = \frac{f\bar{\theta}}{g}\frac{[M]}{[\theta]} \quad , \quad \frac{dz}{dy} = \frac{f\bar{\theta}}{g}\frac{[N]}{[\theta]} \tag{37}$$

Typical values of the slope are 1 in 50 to 1 in 150. Write the angle as α. Transform axes locally to (X,Y,Z) with the Y axis horizontal and parallel to the front, the Z axis normal to the front. Let corresponding velocity components be (U,V,W). The geometry of the front allows us to neglect its curvature to a first approximation, (Hoskins and Bretherton (1972)). Then the scale in the Z direction becomes arbitrarily small and so (10) and (12) imply that ϕ is continuous across the front and (13) implies that there is no flow across the front. These two conditions must determine the position of the front. They are consistent with the conditions satisfied at a discontinuity in the solution of the outer problem.

Inspection of Figs 1 and 2 shows that the scale in the X direction, which is parallel to the front in the plane of the cross-section, will be of the order 100 km, while the scale parallel to the cross-section is of order 1000 km. The continuity equation (13) then requires that U is an order of magnitude less than V; remembering that the origin moves with the front. Substitution into the X and Y momentum equations then gives at O(1)

$$\frac{\partial \phi}{\partial X} - fV\cos\alpha + g\theta/\bar{\theta}\sin\alpha = 0 \tag{38}$$

$$\frac{DV}{Dt} + \frac{\partial \phi}{\partial Y} + fU = 0 \tag{39}$$

These equations are consistent with the outer equations (23) because (38) states that $V = V_g$ and (37) then becomes

$$\frac{DV_g}{Dt} + \frac{\partial \phi}{\partial Y} + fU = 0$$

which is the same as (23). Thus the fronts derived as solutions of the outer equations are self consistent. Similarity solutions of (36) and (37) have been obtained by Hoskins and Bretherton (1972) and others.

The difficulty with this scaling is near the intersection of the front with the boundary. In this region the scale in X becomes much smaller and the balance in the continuity equation is between $\partial U/\partial X$ and $\partial W/\partial Z$, rather than $\partial V/\partial Y$. Under these conditions (38) is no longer accurate. However, in this region frictional effects are also important. The detailed scaling presented by Hoskins and Bretherton suggests that frictional effects become important before DU/Dt becomes of the same order as the terms in (38). If this is the case, and frictional effects are modelled by a viscous term, then the appropriate solution at the intersection with the boundary will be a standard corner flow (Batchelor (1967), p.226).

The correctness of the solution at the intersections with the boundary is probably of critical importance. The solution of the outer equations shown in Fig. 5 has removed fluid initially in contact with the boundary from the boundary. This can be made consistent with the Navier-Stokes equations with no slip boundary conditions by replacing the discontinuity by a shear layer. However, it shows that the outer equations cannot satisfy as many boundary conditions as even the complete inviscid equations (10) to (15). The computational evidence presented in the next section suggests that the effect of this difference in allowable boundary conditions may be very important for the finite difference computations.

To complete the solution it is necessary to insert viscous shear layers at the boundaries and at the internal discontinuity. The first problem has been studied by Wu and Blumen (1982), the second has not yet been treated.

6. Finite difference solutions

We compare the solution of the outer equations (18) to (24) given in Fig. 5 obtained by geometrical methods with finite difference solutions of both the outer equations (Fig. 6), and of the unscaled equations (10) to (15), (Fig. 7). These solutions are referred to as A, B and C. The finite difference solutions were obtained using uniform 200 x 20 grids and standard second order accurate centred differences. Artificial viscous terms were added to capture the jumps as linear terms of the form $K\partial^2\theta/\partial x^2$. The use of diffusion in the y direction as well had negligible effect because of the different resolution in that direction. In solving (18) to (26) it is necessary to calculate $(u_1 v_1 w_1)$ implicitly. This was done by an iterative method described in detail by Cullen and Purser (1984).

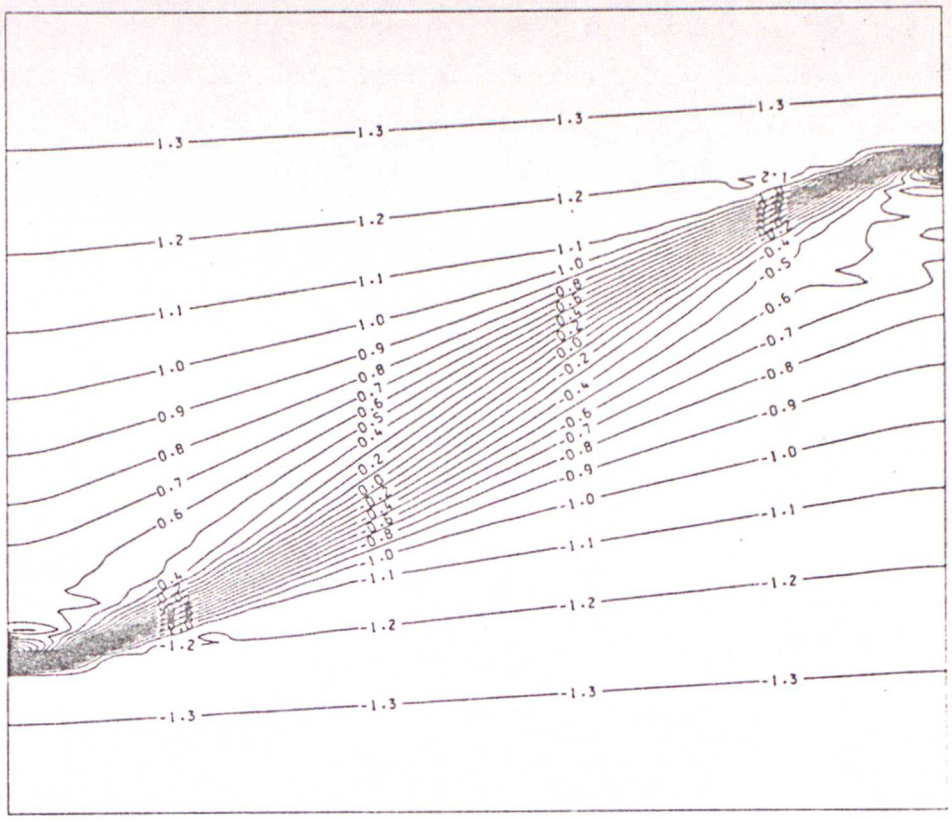

Fig. 6 Finite difference solution of equations (18) to (26), θ field.

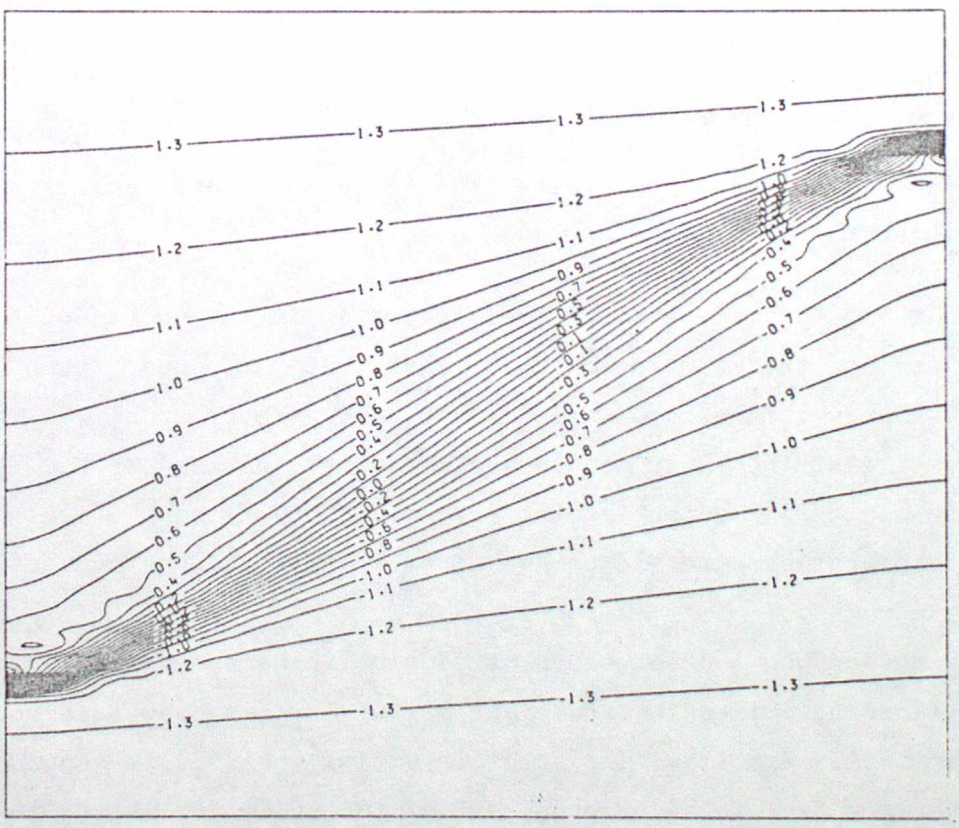

Fig. 7 Finite difference solution of equations (10) to (15), θ field.

Figs. 6 and 7 show the two finite difference solutions to compare with Fig. 5. Neither solution produces sufficient variation of the slope in the isentropes through the depth of the fluid. Experiments using high resolution produced only very slow improvement in this aspect of the solutions. Differences between the two finite difference solutions are shown in Fig. 8.

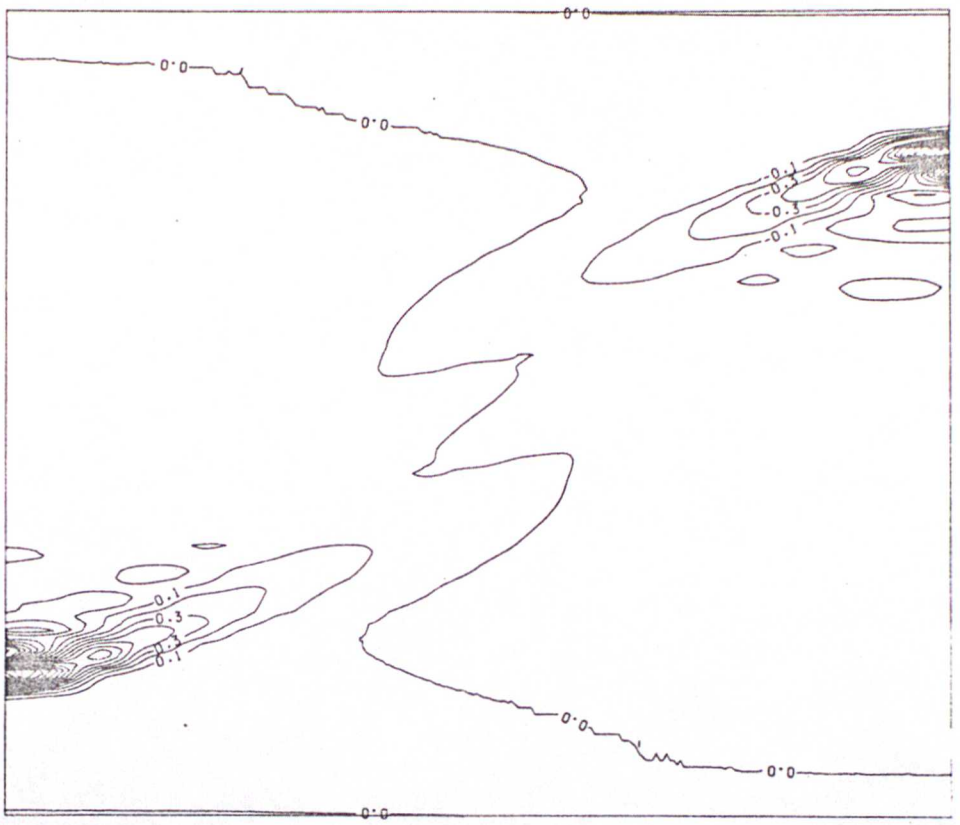

Fig. 8 Difference between the finite difference solutions, solution C minus solution B

This diagram shows that there is little difference in the centre of the region where the slopes of the isentropes are similar, but that, near the boundaries, these slopes change little in C while they become steeper in B. The differences are thus negative at the lower boundary and positive at the upper. This indicates the change in slope with height is better captured by B than C. There is also closer agreement between the slopes away from the frontal surface between A and B than between A and C.

A further check on the solutions is to see if the computed solution, C, of the unscaled equations satisfies the scale analysis. In this case this would require (18) to be satisfied exactly. The error in satisfying (18) is shown in Fig. 9. The largest errors are of the order of 10% of the individual terms in (18).

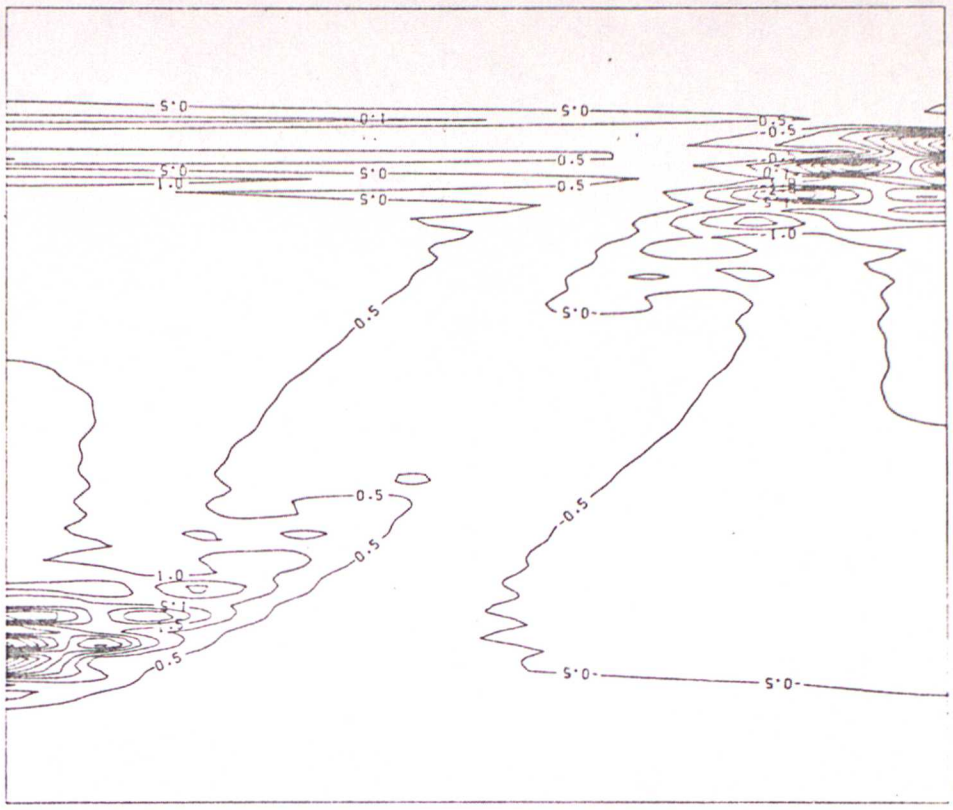

Fig. 9 Difference between fv and $\partial\Phi/\partial x$ in solution C

This suggests either that a straightforward finite difference integration of the equations cannot accurately pick up the solution with the required scaling, or that the solution derived by the scaling arguments is deficient. If the first explanation is correct, then it suggests that improved integration procedures, perhaps enforcing the scaling a priori, are needed for such problems. The difference can also be visualised in terms of the boundary conditions. Solution C appears to retain the condition that fluid initially next to the boundary stays there, at the expense of satisfying (18). Solution B has to satisfy (18), and so has to try and remove fluid from the boundary. The detailed structure of the front is controlled by the artificial viscosity, but that given by B is the closer to A.

Acknowledgements Much of the theoretical work described was done in collaboration with R J Purser. C A Parrett and S Chynoweth assisted with the computer runs. The scaling arguments incorporate a summary of work done at the Oxford Study Group with Industry in March 1984.

References:

G K Batchelor 'An Introduction to Fluid Dynamics', Cambridge University Press, 1967.

A Buzzi and S Tibaldi Quart. J. Roy. Meteor. Soc. 104, 271-288 (1978).

M J P Cullen and R J Purser To appear in J. Atmos. Sci. (1984).

G J Haltiner and R T Williams 'Numerical Prediction and Dynamic Meteorology', 2nd ed., Wiley, New York, 1980.

B J Hoskins Quart. J. Roy. Meteor. Soc. 100, 480-482 (1974).

B J Hoskins Ann. Rev. Fluid. Mech 14, 131-151 (1982).

B J Hoskins and F P Bretherton, J. Atmos. Sci. 29, 11-37 (1972).

B J Hoskins and I Draghici, J. Atmos. Sci. 34, 1859-1867 (1977).

L W Uccellini, P J Kocin, R A Petersen, C H Wash and K F Brill, U.S. Mon. Weath. Rev. 112, 31-55 (1984).

R Wu and W Blumen, J. Atmos. Sci. 39, 1774-1782 (1982).